Inorganic Chemistry

Article

pubs.acs.org/IC

Iridium(III) Hydrido N-Heterocyclic Carbene–Phosphine Complexes as Catalysts in Magnetization Transfer Reactions

Marianna Fekete, Oliver Bayfield, Simon B. Duckett,* Sam Hart, Ryan E. Mewis, Natalie Pridmore, Peter J. Rayner, and Adrian Whitwood

Department of Chemistry, Centre for Hyperpolarization in Magnetic Resonance, University of York, York Science Park, York, YO10 5NY, U.K.

Supporting Information

ABSTRACT: The hyperpolarization (HP) method signal amplification by reversible exchange (SABRE) uses *para*-hydrogen to sensitize substrate detection by NMR. The catalyst systems $[Ir(H)_2(IMes)(MeCN)_2(R)]BF_4$ and $[Ir(H)_2(IMes)(py)_2(R)]BF_4$ [py = pyridine; R = PCy_3 or PPh_3; IMes = 1,3-bis(2,4,6-trimethylphenyl)imidazol-2-ylidene], which contain both an electron-donating N-heterocyclic carbene and a phosphine, are used here to catalyze SABRE. They react with acetonitrile and pyridine to produce $[Ir(H)_2(NCMe)(py)(IMes)(PPh_3)]BF_4$ and $[Ir(H)_2(NCMe)(py)(IMes)(PCy_3)]BF_4$, complexes that undergo ligand exchange on a time scale commensurate with observation of the SABRE effect, which is illustrated here by the observation of both pyridine and acetonitrile HP. In this study, the required symmetry breaking that underpins SABRE is provided for by the use of chemical inequivalence rather than the previously reported magnetic inequivalence. As a consequence, we show that the ligand sphere of the polarization transfer catalyst itself becomes hyperpolarized and hence that the high-sensitivity detection of a number of reaction intermediates is possible. These species include $[Ir(H)_2(NCMe)(py)(IMes)(PPh_3)]BF_4$, $[Ir(H)_2(MeOH)(py)(IMes)(PPh_3)]BF_4$, and $[Ir(H)_2(NCMe)(py)_2(PPh_3)]BF_4$. Studies are also described that employ the deuterium-labeled substrates CD_3CN and C_5D_5N, and the labeled ligands $P(C_6D_5)_3$ and IMes-d_{22}, to demonstrate that dramatically improved levels of HP can be achieved as a consequence of reducing proton dilution and hence polarization wastage. By a combination of these studies with experiments in which the magnetic field experienced by the sample at the point of polarization transfer is varied, confirmation of the resonance assignments is achieved. Furthermore, when $[Ir(H)_2(pyridine\text{-}h_5)(pyridine\text{-}d_5)(IMes)(PPh_3)]BF_4$ is examined, its hydride ligand signals are shown to become visible through *para*-hydrogen-induced polarization rather than SABRE.

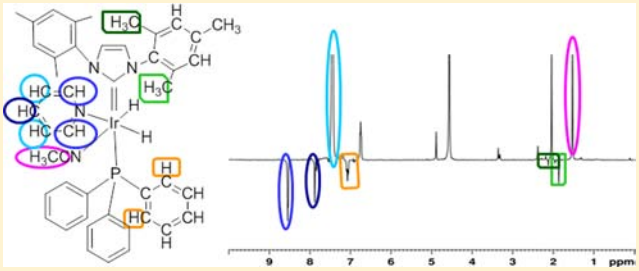

INTRODUCTION

Hyperpolarization (HP) methods are being used to improve the sensitivity of NMR and magnetic resonance imaging to substrate detection.[1] Signal amplification by reversible exchange (SABRE) corresponds to one such method in which the nuclear spin order from *para*-hydrogen (p-H_2) is used to sensitize a substrate. In this case, the process does not involve a change in the chemical structure of the hyperpolarized substrate, as demonstrated in the more traditional p-H_2-induced polarization (PHIP) technique pioneered by Weitekamp and Eisenberg.[2−4] In PHIP, detection of a product that contains two nuclei that were originally located in a single p-H_2 molecule is achieved and therefore a simultaneous change in the chemical identity is required. Nonetheless, this approach is very powerful, and detection of the true reaction intermediates has been achieved,[5−7] the development of NMR theoretical approaches facilitated,[8,9] and the monitoring of hydrogenation products in organic transformation enabled.[10,11] The latter situation has led to significant interest in PHIP as a tool for the in vivo monitoring of living systems.[12] Furthermore, more recently, Koptyug et al. have used the same methods to follow a number of heterogeneous reactions.[13−15]

In SABRE, while the HP feedstock is still p-H_2, a catalyst is now used as a scaffold to temporarily bind both H_2 and the substrate.[16,17] Consequently, after ligand dissociation, there is no change in the chemical identity of the hyperpolarized species. Earlier studies used $[Ir(COD)(PCy_3)(py)]BF_4$, which contains the sterically bulky electron-donating phosphine PCy_3 as a suitable catalyst.[17] More recently, greater HP efficiency has been demonstrated for the related 1,3-bis(2,4,6-trimethylphenyl)imidazol-2-ylidene (IMes) complex, $[Ir(COD)(IMes)Cl]$.[18] Recent reviews illustrate the context of both SABRE and PHIP.[19,20]

The iridium–phosphine system $[Ir(COD)(PCy_3)(py)]^+$ is known as Crabtree's catalyst and is usually associated with a role as either a hydrogenation or deuterium-transfer catalyst.[21] Evidence obtained through studies of the effect of the ligand electronic parameters by Tolman,[22] computation,[23] and

Received: July 16, 2013
Published: November 11, 2013

   dx.doi.org/10.1021/ic401783c | *Inorg. Chem.* 2013, 52, 13453−13461

calorimetric analysis of the bond strengths[24] has revealed that N-heterocyclic carbenes (NHCs) are more electron-donating than phosphines.[25] Furthermore, the work of Nolan and Buriak has shown that the stability and activity of Crabtree's catalyst can be improved with such ligands.[26] They achieve this by combining a bulky NHC, such as IMes, with an appreciably encumbered phosphine (PPh_3, PBn_3, PMe_2Ph, and $PnBu_3$) to deliver the most robust and effective deuterium exchange catalyst.[27]

Upon reaction of $[Ir(COD)(PCy_3)(py)]BF_4$ with pyridine and *p*-H_2, $[Ir(H)_2(PCy_3)(py)_3]BF_4$ formed and proved to function very effectively as a SABRE catalyst.[17] Indeed, measurements under SABRE with its counterpart $[Ir(H)_2(IMes)(py)_3]Cl$ yielded proton signal intensity gains in free pyridine of greater than 3000-fold.[18] These complexes completed the HP transfer step in a low magnetic field in order to facilitate the interactions necessary for spin-order transfer.[8] A growing number of studies have used the SABRE effect.[28−34] Both of these systems are examples of catalysts in which it is magnetic inequivalence in the equatorial plane that provides the necessary symmetry breaking that activates the two nuclei that were originally located within *p*-H_2 and now reside on the metal as a pair of dihydride ligands. Hence while these systems contain three potential polarization acceptors in the form of pyridine, only the two that are trans to hydride fulfill this role and, consequently, the effective spin system involved in transfer is made up of just 2 hydride and 10 pyridine protons. We aim here to show that it is possible to improve on the efficiency of this polarization transfer catalyst by sharing the *p*-H_2 spin order with fewer protons. While this has already been demonstrated by using deuterated substrates,[18,35] a redesign of the catalyst to include fewer exchangeable ligand sites offers another route to achieving this goal. In this paper, we describe how the combination of an electron-donating NHC and a phosphine produces a new set of high-activity catalysts for SABRE. The phosphines employed are PCy_3 and PPh_3, and they provide access to the well-defined complexes $[Ir(H)_2(IMes)(MeCN)_2(PPh_3)]BF_4$ and $[Ir(H)_2(IMes)(MeCN)_2(PCy_3)]BF_4$. The molecules that are hyperpolarized in this study correspond to pyridine and acetonitrile. It has previously been suggested that the HP efficiency of the SABRE catalyst is linked to both the lifetime of the metal complex and the strength of the magnetic field where polarization transfer occurs.[8] These concepts are further tested here by using a *flow*-polarization apparatus that has been previously described.[18,36] In particular, we explore the ligand-exchange processes and demonstrate how a number of new species are detectable, including characterization of a C−H bond activation product that acts as a resting state within the SABRE process. In this case, it is products of the type $[Ir(H)_2(NCMe)(py)(IMes)(PR_3)]BF_4$ that are dominant in the catalyst medium. The effect of the magnetic field experienced by the catalyst at the point of polarization transfer (the polarization transfer field, or PTF) is monitored experimentally and shown to vary with the identity of the catalyst and detected substrate. We also demonstrate how breaking of the original *p*-H_2 molecule symmetry through the chemical shift difference in the dihydride product $[Ir(H)_2(NCMe)(py)(IMes)(PR_3)]BF_4$ enables the wide transfer of HP within the parent complex and hence their detection as examples of hyperpolarized reaction intermediates.

EXPERIMENTAL SECTION

$[Ir(COD)(PCy_3)(py)]PF_6$ (**1**) was obtained from Strem. $[Ir(COD)\{CO(CH_3)_2\}(IMes)]BF_4$ (**2**), $[Ir(H)_2(NCMe)_2(IMes)(phosphine)]BF_4$ (**3a** and **4a**), $[Ir(H)_2(py)_2(IMes)(PPh_3)]BF_4$ (**3b**), and $[Ir(H)_2(NCMe)(py)(IMes)(PPh_3)]BF_4$ (**3c**) were prepared based on published literature methods, as described in the Supporting Information.[37] All NMR measurements were recorded on a Bruker Avance III series 400 or 500 MHz system. Samples were now typically dissolved in 3 mL of methanol-d_4 (5 mM) and contained pyridine (5 or 20-fold excess). Single crystals of both **3c** and **5** were grown from a benzene solution and analyzed on an Oxford Diffraction SuperNova diffractometer. The crystals were kept at 110.00(10) K during data collection.

$[Ir(H)_2(NCMe)_2(IMes)(PPh_3)]BF_4$ (3a). ^1H NMR (400 MHz, $CDCl_3$, 298 K): δ −21.45 (d, 2H, J_{HP} = 17.27 Hz), 1.65 (s, 6H, $NCCH_3$), 2.11 (s, 12H, CH_3 of IMes), 2.38 (s, 6H, CH_3), 6.95−7.34 (m, 21H, CH, PPh_3, IMes). $^{13}C\{^1H\}$ NMR (101 MHz, $CDCl_3$, 298 K): δ 1.0 ($NCCH_3$), 17.9, 21.2 (CH_3), 117.83 (NCMe), 122.2, 122.6 (NCH), 127.9, 128.9, 129.6 (d, CH, J_{CP} = 11.3 Hz), 129.8, 132.7, 133.1 (CH), 133.9, 134.4 6 (d, CH, J_{CP} = 11.0 Hz), 135.9, 137.6, 138.8 (−C═), 164.1 (d, NCN, J_{CP} = 114.7 Hz). $^{31}P\{^1H\}$ NMR (162 MHz, $CDCl_3$, 298 K): δ 18.96. ^{11}B NMR (160 MHz, CD_3CN, 298 K): δ −1.40 ($^{11}BF_4$, 81%), −1.42 ($^{10}BF_4$, 19%). ^{19}F NMR (470 MHz, CD_3CN, 298 K): δ −152.89 ($^{10}BF_4$, 19%), −152.94 ($^{11}BF_4$, 81%). ESI MS: 802.29 [M^+ − NCMe].

Compound 3b. ^1H NMR (400 MHz, methanol-d_4, 296 K): δ −22.74 (d, 2H, J_{HP} = 18.4 Hz), 1.97 (s, 12H, CH_3 of IMes), 2.31 (s, 6H, CH_3), 6.75−7.29 (m, 27H, CH, PPh_3, IMes, py), 7.55 (t, 2H, J_{HH} = 7.2 Hz, para ^1H py), 7.55 (d, 4H, J_{HH} = 4.5 Hz, ortho ^1H py). $^{13}C\{^1H\}$ NMR (101 MHz, methanol-d_4, 298 K): δ 17.9, 21.2 (CH_3), 122.0, 122.3 (NCH), 123.6 (CH, py), 127.8, 128.7, 129.5 (d, CH, J_{CP} = 11.3 Hz), 129.7, 132.5, 133.1 (CH), 133.9, 134.4, (d, CH, J_{CP} = 11.0 Hz), 135.7 (CH, py), 135.9, 137.6, 138.8 (−C═), 149.7 (−C═, py), 164.1 (d, NCN, J_{CP} = 114.7 Hz). $^{31}P\{^1H\}$ NMR (162 MHz, methanol-d_4, 298 K): δ 22.1. ESI MS: 840.31 [M^+ − py].

Compound 3c. This complex was prepared in situ in an NMR tube by adding 5 equiv of acetonitrile to a solution of **3b** or 5 equiv of pyridine to a solution of **3a**. ^1H NMR (500 MHz, acetonitrile-d_3, 298 K): δ −22.30 (dd, 1H, trans to pyridine, J_{HH} = 7.21 Hz, J_{HP} = 19.44 Hz), −21.10 (dd, 1H, trans to $NCCH_3$, J_{HH} = 7.21 Hz, J_{HP} = 16.09 Hz), 1.52 (s, 3H, coordinated $NCCH_3$), 1.80 (s, 6H, CH_3), 2.00 (s, free $NCCH_3$), 2.15 (s, 6H, 2 × $-CH_3$), 2.36 (s, 6H, 2 × $-CH_3$), 6.81 (d, 1H, −CH═, J_{HH} = 0.77 Hz), 6.97 (d, 1H, CH, J_{HH} = 0.77 Hz), 7.05−7.49 (m, 21H, CH, PPh_3, IMes), 7.78 (t, 1H, para ^1H pyridine), 8.72 (d, 2H, ortho ^1H pyridine. $^{31}P\{^1H\}$ NMR (161 MHz, CD_3CN, 298 K): δ 22.98. ^{11}B NMR (160 MHz, CD_3CN, 298 K): δ −1.05. ^{19}F NMR (470 MHz, CD_3CN, 298 K): δ −154.69 ($^{10}BF_4$, 19%), −154.74 ($^{11}BF_4$, 81%). ^{15}N NMR (40.54 MHz, $CDCl_3$, 263 K): δ 177.8 (coordinated $NCCH_3$), 195.8 (NCN, IMes), 238.1 (coordinated pyridine).

$[Ir(H)_2(NCMe)_2(IMes)(PCy_3)]BF_4$ (4a). ^1H NMR (400 MHz, methanol-d_4, 296 K): δ −22.24 (d, 2H, J_{HP} = 18.7 Hz), 1.32−1.96 (m, 30H CH_2 of PCy_3), 2.16 (s, 6H, CH_3 of acetonitrile), 2.21 (s, 12H, CH_3 of IMes), 2.38 (3H, m, CH of PCy_3), 7.08 (m, 2H, CH, IMes. $^{13}C\{^1H\}$ NMR (101 MHz, $CDCl_3$, 298 K): δ 1.4 ($NCCH_3$), 16.0, 19.8 (CH_3), 25.8, 26.2, 27.0, 28.4, 30.5, 32.8, 33.1 (CH_2), 118.8 (NCMe), 122.5, 125.1 (NCH), 128.5 (CH), 135.8, 137.9, 138.5 (−C═), 173.9 (d, NCN, J_{CP} = 118.0 Hz). $^{31}P\{^1H\}$ NMR (162 MHz, methanol-d_4, 296 K): δ 18.24. ESI MS: 779.40 [M^+ − 2NCMe].

NMR Data for $[Ir(H)_2(py)_2(IMes)(PCy_3)]BF_4$ (4b). ^1H NMR (400 MHz, methanol-d_4, 296 K): δ −23.83 (d, 2H, J_{HP} = 18.7 Hz), 1.32−1.96 (m, 30H, CH_2 of PCy_3), 2.19 (s, 12H, CH_3 of IMes), 2.41 (s, 6H, CH_3 of IMes), 7.21 (s, 4H, CH, IMes), 7.66 (t, 2H, meta ^1H pyridine), 8.01 (s, 2H, CH, IMes), 8.18 (t, 1H, para ^1H pyridine), 8.95 (d, 2H, ortho ^1H pyridine). $^{31}P\{^1H\}$ NMR (162 MHz, methanol-d_4, 298 K): δ 21.9.

NMR Data for $[Ir(H)_2(NCMe)(py)(IMes)(PCy_3)]BF_4$ (4c). ^1H NMR (400 MHz, methanol-d_4, 296 K): δ −23.42 (dd, 1H, J_{HP} = Hz), −21.98 (dd, 1H, J_{HP} = Hz), 1.13−1.73 (m, 30H, CH_2 of PCy_3), 1.83

dx.doi.org/10.1021/ic401783c | Inorg. Chem. 2013, 52, 13453−13461

Scheme 1. Equilibration of 3a or 3b with Pyridine and Acetonitrile Leading to 3c as the Dominant Product

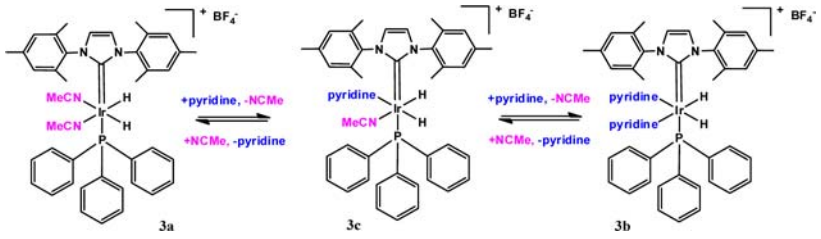

(s, 6H, CH_3 of IMes), 2.15 (s, 6H, CH_3 of IMes), 2.19 (s, 3H, CH_3, acetonitrile), 2.38 (s, 6H, CH_3 of IMes), 6.90 (s, 2H, −C*H*═, IMes), 7.07 (s, 2H, −C*H*═, IMes), 7.16 (t, 2H, J_{HH} = 6.3 Hz, meta ^{1}H pyridine), 7.18 (s, 2H, −C*H*═, IMes), 7.81 (t, 1H, J_{HH} = 8.3 Hz, ortho ^{1}H pyridine), 8.23 (d, 2H, J_{HH} = 4.3 Hz, para ^{1}H pyridine). ^{31}P{^{1}H} NMR (162 MHz, methanol-d_4, 298 K): δ 22.73.

RESULTS AND DISCUSSION

Complexes **3a**, **3b**, and **4a** were prepared and characterized by multinuclear NMR spectroscopy. Key resonances are listed in the Experimental Section. The hydride ligands in these species appear as simple phosphorus-coupled doublets at δ −21.40, −22.70 and −22.24, in methanol-d_4 at 298 K and at δ −21.45, −22.80, and −22.42 in $CDCl_3$. These resonances are used to monitor the chemical evolution of these systems as they react with pyridine and acetonitrile. Two control samples were prepared to do this. The first sample contained **3a** in methanol-d_4 and 5 equiv of pyridine and 3 bar of H_2. The second contained **3b** in $CDCl_3$ and 1 equiv of NCMe and 3 bar of H_2. In both cases, the hydride signals of **3a** or **3b** were replaced by a common species that yielded a pair of coupled hydride ligand signals at δ −21.02 and −22.18. This product, **3c**, is the sole product in both reactions and confirms that **3c** is thermodynamically more stable than either **3a** or **3b**, as illustrated by Scheme 1 and Figure 1.

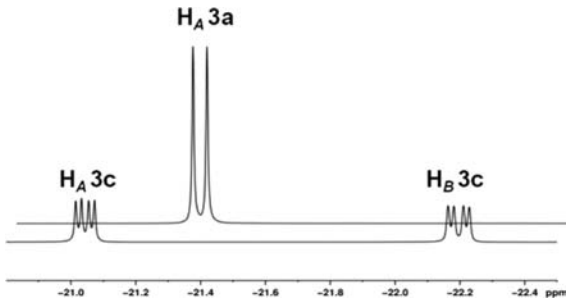

Figure 1. Hydride region of two ^{1}H NMR spectra used to illustrate the conversion of **3a** into **3c** upon the addition of pyridine. These traces were recorded at 273 K in $CDCl_3$.

The peak integrals for these two hydride resonances of **3c** exhibit the expected 1:1 ratio, and we note that a coordinated NCMe signal appears at δ 1.48. In **3c**, the methyl substituents of the IMes ligand appear as three distinct sets, each of six protons, in accordance with rapid rotation about the metal−carbene and N−C bonds (see the Experimental Section). The hydride ligand resonances of **3c** are also well-resolved and connect, according to nuclear Overhauser effect methods, with proton signals at δ 6.99 and 1.48, which are attributed to bound pyridine and CH_3CN ligands, respectively. These connections arise because of through-space interactions and confirm the cis-ligand arrangement that is shown in Figure 1. In contrast, when a ^{1}H−^{15}N HMQC NMR spectrum is recorded for this system (in $CDCl_3$), where the ^{15}N label is present at natural abundance, as shown in Figure 2, a different set of connections

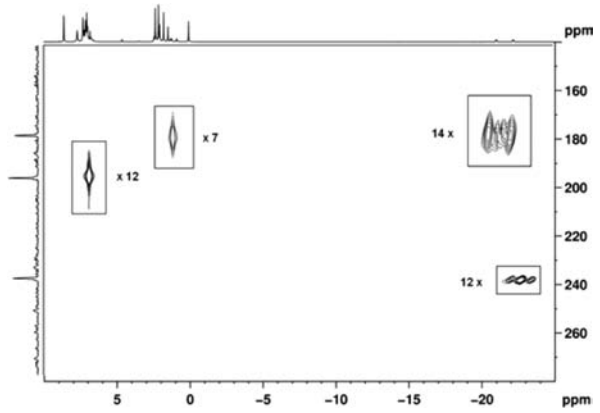

Figure 2. 2D ^{1}H−^{15}N HMQC NMR spectrum of unlabeled **3c** recorded at 263 K in $CDCl_3$, with the resulting ^{15}N data providing diagnostic information on the ligand arrangement, as discussed in the text (relative expansions in the boxed areas are indicated).

become visible. Now the hydride signal that appears at lower field connects with a coordinated acetonitrile ^{15}N signal at δ 177.8 through a 15.3 Hz J_{H15N} splitting; it also connects to its CH_3 partner at δ 1.48. The second, higher field, hydride signal at δ −22.18 possesses a J_{HN} splitting of 18.5 Hz and is located trans to pyridine. The ^{15}N resonance of the associated coordinated pyridine ligand of **3c** appears at δ 239.1 in this NMR spectrum. In addition to these two connections, the δ 6.99 (J_{HN} = 10.6 Hz) signal of the −CH═CH− protons in the imidazolium ring of the IMes ligand shows a strong correlation peak to a third ^{15}N signal at δ 195.7 in this experiment. These measurements therefore locate key ^{15}N ligand resonances in **3c** and give a high level of confidence in our product assignment; we note that these measurements were achieved in only a few hours without ^{15}N labeling. The characterization of **3c** was further confirmed by X-ray crystallography at 110 K. Figure 3 shows the corresponding ORTEP for **3c**, while Table 1 lists key bond lengths and angles.

Characterization of 4c. A series of related studies were then undertaken on the PCy_3 analogues of **3**. These studies revealed that, upon dissolution of **4a** in methanol-d_4 and the addition of 5 equiv of pyridine and 3 bar of H_2, **4c** was formed in a manner similar to that of **3c**. NMR data for **4a**−**4c** are presented in the Experimental Section.

It is well-known that species such as **3c** and **4c** can undergo C−H activation of an *o*-methyl group of the mesityl ring after ligand loss. Aldridge and co-workers[38] reported such an observation in the solid-state chemistry of Ir(IMes)(IMes′)(H)Cl, while Torres et al.[37] demonstrated that [Ir(H)$_2$(IMes)-

dx.doi.org/10.1021/ic401783c | Inorg. Chem. 2013, 52, 13453−13461

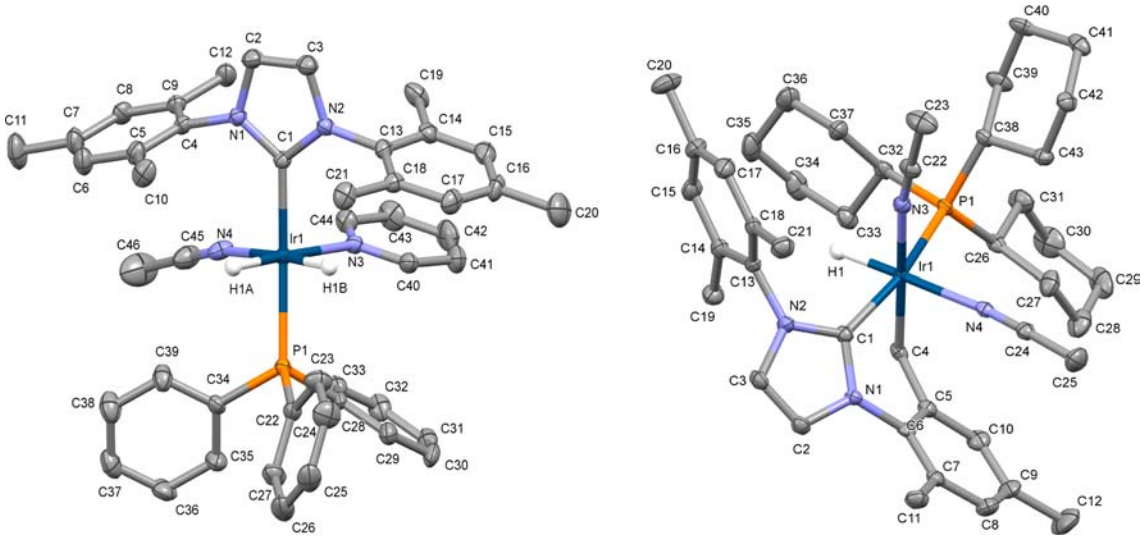

Figure 3. ORTEP diagrams of the cations **3c** and **5** as determined by X-ray diffraction.

Table 1. Bond Distance (Å) and Angles (deg) for Complexes 3c and 5

	3c	5
Ir−P1	2.2832(9)	2.3347(9)
Ir−H1	1.603	1.604
Ir−C1	2.068(4)	2.046(3)
Ir−C4		2.101(3)
Ir−N3	2.160(3)	2.090(3)
Ir−N4	2.107 (5)	2.154(3)
C1−Ir−P1	168.29(11)	165.48(10)
C4−Ir−P1		94.00(10)
C1−Ir−C4		80.24(13)
N3−Ir−N4	91.6(2)	85.55(11)
N3−Ir−H1	176.58	
N4−Ir−H1	175.85	179.16
N3−Ir−C1	93.96(13)	94.82(12)
N4−Ir−C4	97.54(14)	92.06(12)01
P1−Ir−N3	94.14(7)	91.41(8)
P1−Ir−N4	90.67(11)	100.54(8)

$(NCMe)_2(P^iPr_3)]PF_6$ forms $[IrH(IMes')(NCMe)_2(P^iPr_3)]PF_6$ upon treatment with ethylene. In this case, upon exposure of the cyclometalated complex to H_2, the dihydride is re-formed. We were therefore not surprised when a sample of **4a** that was placed under N_2 underwent H_2 reductive elimination to form a new product. This species proved to correspond to $[IrH(IMes')(NCMe)_2(PCy_3)]BF_4$ (**5**). Isolation of complex **5** led to the collection of X-ray-quality crystals, which yielded the structure shown in Figure 3. The Ir−phosphine bond lengths in **5** and the related complex $[IrH(IMes')(NCMe)_2(P^iPr_3)]PF_6$ are 2.3347(9) and 2.3367(17) Å and hence indistinguishable. In contrast, the corresponding Ir=C_1 bond lengths are slightly different at 2.046(3) vs 1.973(7) Å, in accordance with the greater electron-donating power of PCy_3 vs P^iPr_3. The corresponding Tolman cone angles change from 170° to 160° for these ligands. The difference in the phosphine steric bulk changes the structure such that in **5** the equatorial N−Ir−C and N−Ir−H bond angles are larger than those for $[IrH(IMes')(NCMe)_2(P^iPr_3)]PF_6$.

Kinetics of Ligand Exchange in 3c and 4c. It should be clear that the dominant species present in these solutions is **3c** or **4c**. A series of ^{1}H-selective EXSY NMR experiments were therefore performed in order to probe the ligand-exchange processes undergone by **3c** and **4c**. These data are presented in the Supporting Information (section 4), but our findings are summarized here. In the first instance, **3c** was observed to undergo magnetization transfer between free and bound pyridine, free and bound acetonitrile, and the two hydride sites, as illustrated in Scheme 2. When the experimentally observed rate of transfer of magnetization from bound pyridine into free pyridine was monitored as a function of the pyridine concentration, saturation behavior indicative of a dissociative process was evident at high pyridine concentrations. The limiting rate constant for magnetization transfer into free pyridine was determined to be 1.15 ± 0.1 s^{-1}. However, when a similar sample was examined, where the initial concentrations of **3c** and pyridine were 0.0152 and 0.0342 M, respectively, the rate of magnetization transfer into free pyridine reduced to zero with increase in the acetonitrile concentration. This information suggests that it is actually acetonitrile dissociation that accounts for the observed pyridine magnetization transfer. Hence, this process happens by secondary ligand exchange through unstable **3b** as indicated in Scheme 2 rather than the direct dissociation of pyridine. This deduction was confirmed when the effect of the acetonitrile concentration on the rate of transfer of bound to free acetonitrile was explored. Now exchange rate saturation was again seen, but the maximum rate constant for ligand loss proved to be 1.95 ± 0.1 s^{-1}. This value is twice that of the limiting pyridine rate, a link that is expected if **3b** were to be involved because once formed there is now an equal probability of losing the magnetically labeled pyridine or the freshly bound pyridine ligand. Furthermore, the observed rate constant for hydride site interchange is smaller than this and is affected by the ligand excess, in accordance with the 16-electron reaction intermediate retaining unique hydride ligand identities as expected.[39]

In contrast, when **4c** is examined, a limiting reaction rate is again reached as both the pyridine and acetonitrile concentrations are increased. However, now the limiting rate constant for pyridine loss is 3.1 ± 0.1 s^{-1}, while that for acetonitrile loss is half that, at 1.4 ± 0.1 s^{-1}. Hence, for **4c**, the mechanism

dx.doi.org/10.1021/ic401783c | Inorg. Chem. 2013, 52, 13453−13461

Scheme 2. Magnetization Transfer Pathways Revealed through EXSY Examination of 3 (R = Ph) or 4 (R = Cy) with Pyridine and Acetonitrile as a Function of the Reagent Concentration[a]

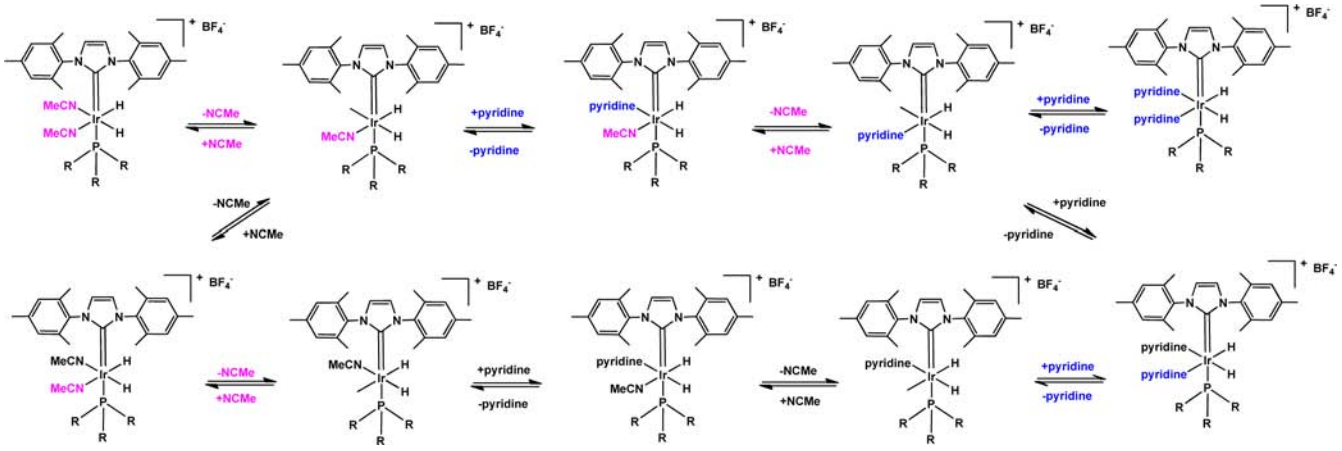

[a]The color scheme shows how labeled magnetization can propagate through the system, based on the indicated dissociative reactions. Solvation of the intermediates is to be expected, and distinct hydride ligand sites are retained in these complexes.

seems to be inverted, with the main ligand loss process corresponding to loss of pyridine. Consequently, trapping with acetonitrile now leads to **4a**, where two identical equatorial ligands reside. The temperature dependence of the observed magnetization transfer rates between the bound and free ligands is detailed in the Supporting Information.

It is interesting to note that when the hydride ligands of **3c** are probed by EXSY spectroscopy, no exchange into free H_2 is observed. This situation marks a significant difference in behavior from that previously reported for **1** and **2**, where H_2 loss is relatively facile. These data therefore suggest that **3c** and **4c** are suitable as SABRE catalysts because they undergo ligand exchange on the NMR time scale. We now describe a series of SABRE-type measurements that are designed to explore this hypothesis.

Using 3 and 4 as SABRE Catalysts. In order to monitor these complexes under SABRE conditions rather than PHIP, a flow apparatus that has been previously described was employed.[36] This equipment allows for the automated collection of hyperpolarized NMR data. A series of identical solutions were prepared, containing the same amount of specified catalyst (**1**, **2**, **3a**, **3b**, and **4a**) and a 20-fold excess of pyridine. The total ^{1}H NMR signal enhancement of the three proton sites of pyridine was then plotted as a function of the strength of the PTF. Table 2 summarizes these data, while Figure 4 illustrates a typical ^{1}H NMR spectrum of the organic region to demonstrate the impact of SABRE and Figure 5 shows the corresponding PTF plot for the signal amplification

Table 2. Total Pyridine Proton Signal Enhancement (Metal Concentration 5.5 mM; 20-Fold Excess of Pyridine) Measured in Conjunction with the Described SABRE–Flow Apparatus for the Indicated PTF with the Corresponding Experimentally Determined Rate of Ligand Loss

catalyst precursor	field/G	absolute value	ligand loss rate constant (s^{-1})
1	40/90	130	0.46
2	110	646	6.26
3a	140	405	1.94
3b	130	372	1.94
4	130	685	3.1

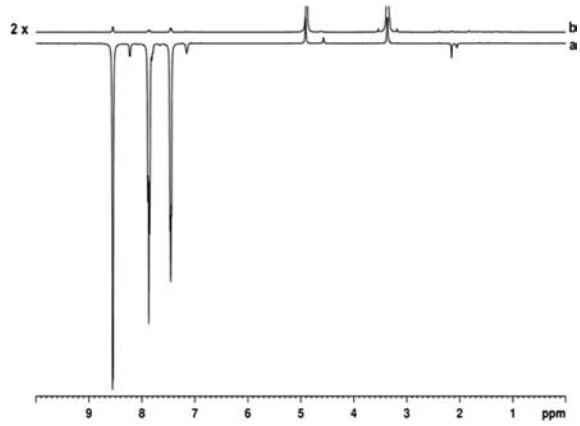

Figure 4. (a) One-scan ^{1}H NMR spectrum showing the hyperpolarized pyridine signals produced under SABRE with **4**. (b) Thermal control spectrum illustrating the scale of signal enhancement.

of the meta resonance of pyridine as a function of the catalyst identity.

Surprisingly, the level of proton signal enhancement observed using **4c** is comparable to that found for **2** even though the ligand-exchange rates are slower. Additionally, the level of signal enhancement seen in the proton signals of acetonitrile, phosphine, and IMes ligands of **4c** is substantial, albeit at a lower level than that of pyridine. We further note that when **3c** and **4c** are employed as magnetization transfer catalysts, transfer into the protons of NCMe is observed. The level of enhancement seen for the acetonitrile protons in these systems reaches a maximum with a PTF of 20 G, as shown in Figure 6.

Exploring the Reactions of 3c and 4c by PHIP. This involved taking a solution of **3a**, with added pyridine, under *p*-H_2, and collecting a ^{1}H NMR spectrum at 298 K using a 45° excitation pulse. Now strong PHIP was seen for the signals that arise from the two hydride ligands of **3c**, as shown in Figure 7. No signals for either **3a** or **3b** were visible in this NMR spectrum, and these data are consistent with the previous section, which detailed how **3c** is the thermodynamic product of the reaction. These NMR spectra, however, do reveal the presence of a further minor reaction product that is not readily

dx.doi.org/10.1021/ic401783c | Inorg. Chem. 2013, 52, 13453–13461

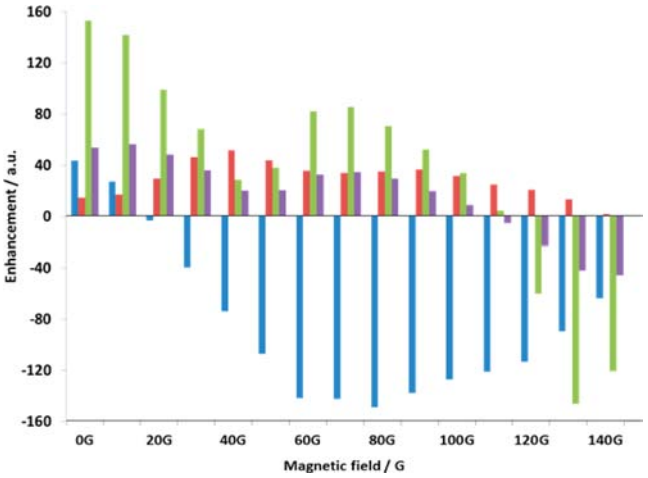

Figure 5. Plot showing how the PTF controls both the degree of pyridine meta proton signal enhancement and the phase of the signal for transfer in a methanol-d_4 solution using **2** (blue), **1** (red), **3c** (purple), and **4c** (green) SABRE catalysts when 1 equiv of NCMe and 20 equiv of pyridine are present in solution.

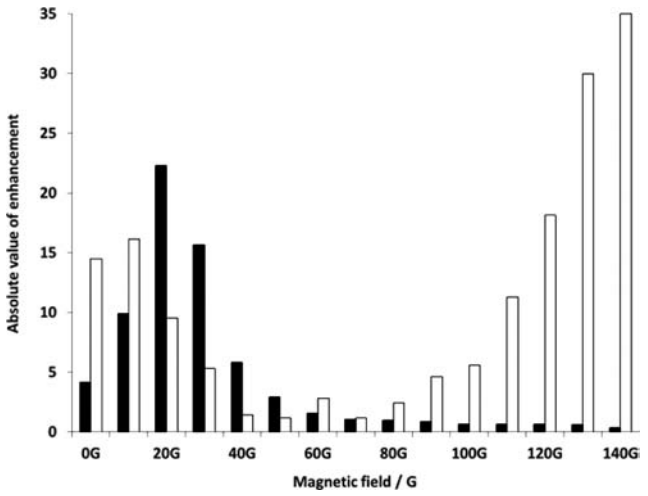

Figure 6. Plot showing the PTF dependence on the absolute signal enhancement observed for the protons of (■) acetonitrile (11-fold excess) and (○) pyridine (31-fold excess), produced in a methanol-d_4 solution using the SABRE catalyst **3c** at 291 K.

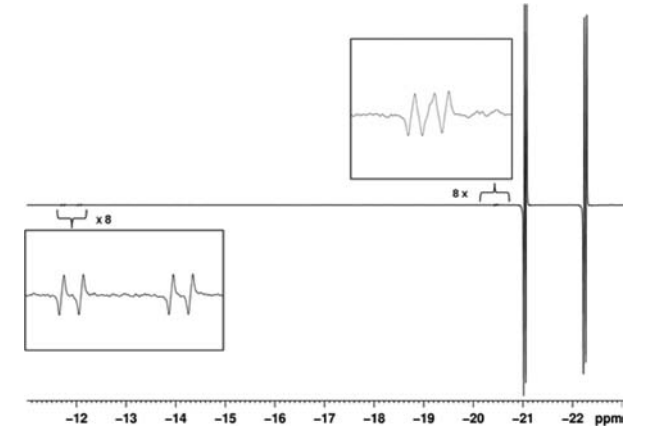

Figure 7. ^{1}H NMR spectrum of the hydride region of a methanol-d_4 solution of **3c** under p-H_2, revealing the pairs of hydride resonances for **3c** (major) and **6** (minor).

visible without PHIP. This product appears as a pair of mutually coupled hydride signals at δ −11.89 (ddd, J_{HH} = 4.8, J_{PcisH} = 23.6, and $J_{PtransH}$ = 133.8 Hz) and δ −20.45 (multiplet, J_{HH} = 4.5, J_{PcisH} = 16.0, and J_{PcisH} = 11.3 Hz), which possess couplings to two inequivalent ^{31}P centers. These centers were located at δ 2.87 (trans to the hydride resonating at δ −11.89) and 6.30 (cis to both hydrides) in the corresponding 2D ^{1}H−^{31}P NMR correlation. The corresponding ^{1}H−^{15}N HMQC NMR experiment revealed that the hydride signal at δ −20.45 connected with an acetonitrile ^{15}N signal at δ 196.7 through a trans coupling. These results confirm that this additional species is the ligand redistribution product $[Ir(H)_2(NCMe)(IMes)(PPh_3)_2]BF_4$ (**6**), with a cis−cis hydride and phosphine ligand arrangement.

Exploring the Reactions of 3c and 4c by SABRE. When an analogous sample was examined using the flow apparatus, after a p-H_2 exposure time of 30 s, the SABRE effect was observed in some of the resonances of **3c** and **6**. For example, the signal for the o-phenyl proton of the phosphine ligand of **3c** now appears as an emission peak, a triplet at δ 7.05, which simplifies upon ^{31}P decoupling into the expected doublet. A weaker signal at δ 6.99 is visible for an o-phenyl proton of the phosphine in **6**. The signal intensities seen for these hyperpolarized ligand resonances proved to vary with the PTF used for SABRE and, in this case, were maximized when set to 50 and 90 G, respectively. The o-pyridine proton signal for **3c** can also be seen as a SABRE-enhanced signal at δ 7.78 in these measurements. Upon examination of the region around δ 2.0, hyperpolarized signals are also detected at δ 2.05, 1.54, and 1.32 for free CH_3CN and bound CH_3CN in **3c** and **6**, respectively. These resonances proved to have maximum intensity when the PTF was 20 G. Additionally, when the PTF field was increased to 140 G, signals for the corresponding methyl protons of the IMes ligands in **3c** and **6** were enhanced; they appear at δ 1.88, 2.13, and 2.39 for **3c** and at δ 2.36 and 3.05 for **6**. These observations have therefore demonstrated that the SABRE effect can be used to observe key resonances in these complexes at high sensitivity. They also reveal that the PTF can be used to select key resonances.

Exploring the Reactions of 3c by SABRE While Employing a Range of Deuterated Ligands. We have built further on these SABRE studies by reexamining these reactions in conjunction with deuterium labeling, with the aim of making the ligand resonances even more intense. For example, when pyridine-d_5, rather than pyridine-h_5, is used, the SABRE-enhanced signals seen for the o-phenylphosphine protons of **3c** and **6** proved to be reduced in intensity by around 80%. In contrast, the corresponding signals for the CH_3CN ligands of **3c** and **6** were, however, now 20% stronger, with the methyl resonances of their IMes groups showing an 8 fold increase under optimum conditions rather than the 4-fold seen in the experiments with pyridine-h_5. The signal enhancements for the hydride ligand signals of **3c** were also increased by 20% over those seen with pyridine-h_5. The effects of deuteration are therefore substantial and confirm that, by a reduction in the number of protons in the spin system, the signal enhancement can be focused onto the remaining resonances. For the phosphine, however, the opposite is true, and hence we can deduce that its signals are actually enhanced via transfer from the protons of pyridine.

Interestingly, when a mixture of pyridine-h_5 and pyridine-d_5 is employed, the hydride ligands of **3b** now become visible as strongly PHIP-enhanced signals. These hydride resonances are

strongly amplified by virtue of the creation of a small chemical shift difference between them; the result of this process is the creation of two AB-type hydride resonances. Consequently, when a 45° excitation pulse is employed, these signals dominate, although the signals for **3c** and **6** are still visible. Under SABRE conditions, enhanced signals for **3b** are also visible at δ 7.09 (the *o*-phenyl proton of the phosphine), at δ 7.98 (the *o*-pyridine proton), and at δ 2.16 for its IMes ligand in this experiment.

Furthermore, when PPh_3-d_{15} is employed instead of PPh_3-h_{15}, the hydride ligand signals of **3c** and **6** appear to be 27% larger and 26% smaller, respectively. One further benefit of deuteration is that the ^{1}H resonances of the bound pyridine-h_5 ligands in these species can now be clearly seen because there is no longer any overlap with what would be PPh_3-h_{15} resonances. The important aspects of this behavior are illustrated in Figure 8. We note, however, that separation of these signals can also be

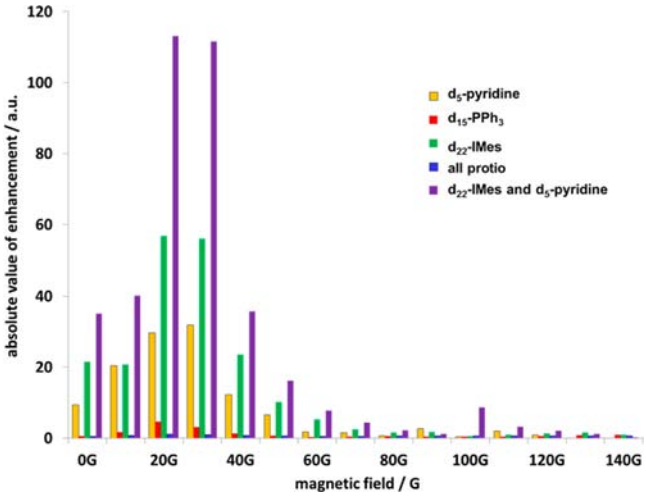

Figure 8. Plot of variation of the NCMe ^{1}H signal intensity versus PTF when a **3c**-derived catalyst system is employed in conjunction with the specified deuterium labeling. A total of 3 mL of a methanol-d_4 solution of **3c** (5.5 mM) with an 11-fold excess of NCMe and a 31-fold excess of pyridine relative to metal was employed in these room temperature measurements.

achieved by varying the PTF and, consequently, either route can be used to confirm the resonance assignment. This means that even if deuteration is not chemically viable, characterization is still possible.

We have also studied the effect of deuteration on the polarization of free NCMe. When pyridine-d_5 was used instead of pyridine-h_5, the enhancement level of the NCMe protons is 25 times higher. Furthermore, if a IMes-d_{22} ligand is used, this increases further to an absolute enhancement of 49-fold. When both IMes-d_{22} and pyridine-d_5 are employed, the enhancement level rises yet further to 117-fold. These data are illustrated in Figure 8 and therefore demonstrate that it is possible to produce a viable NCMe HP transfer catalyst. We note that the cyanide function plays a role in many important drugs such as AstraZeneca's Anastrozole, which is marketed as Arimidex.[40]

We further note that when *p*-H_2 is used to examine the original solution of **3a** in the presence of a very small amount of pyridine (0.1-fold based on iridium) with methanol-h_4 (120-fold) in methanol-d_4, while weak signals for **3a** dominate, PHIP-enhanced signals are seen for both **3c** and **6** in addition to those of two further products. These additional products yield pairs of hydride signals at δ −20.56 (dd, J_{HH} = 6.1 Hz, J_{PH} = 12.9 Hz) and −22.54 (dd, J_{HH} = 5.8, J_{PH} = 18.6 Hz) (**3d**) and at δ −20.81 (dd, J_{PH} = 18 Hz) and δ −21.88 (dd, J_{PH} = 17 Hz) (**3e**). They are therefore both monophosphine-containing. Species **3d** was assigned as $[Ir(H)_2(MeOH)(py)(IMes)(PPh_3)]^+$ on the basis of a series of multinuclear NMR observations. It is worth noting, in the corresponding ^{1}H−^{1}H COSY experiment, the hydride signal of **3d** at δ −20.56 coupled with a hydride signal at δ −22.54 and a $-CH_3$ proton signal of a bound methanol-h_4 ligand at δ 2.99. In the corresponding ^{1}H−^{31}P HMQC NMR experiment, a ^{31}P signal at δ 6.54 was seen for **3d**. In contrast, **3e** is $[Ir(H)_2(NCMe)(py)_2(PPh_3)]^+$, and while its NMR signals are too weak for full characterization, a proton signal of the axial pyridine ligand was located at δ 9.04. In both of the newly detected complexes, **3d** and **3e**, it is the chemical shift of the hydride ligands that secures their identity.

These unusual deductions are supported by Figure 9 where part a shows the one-scan ^{1}H NMR spectrum that was recorded after 30 s of bubbling of *p*-H_2 through a methanol-d_4 solution of **3c** at a PTF of 130 G. In the hydride region of this spectrum, PHIP-enhanced signals are seen for **3a**, **3d**, **3e**, and **6**. In contrast, the organic region shows polarized and diagnostic proton signals for bound PPh_3, the $-CH_3$ groups of the IMes ligands, the pyridine ligands, and the NCMe ligands in these species. When the corresponding ^{1}H OPSY NMR spectrum (Figure 9b) was collected, the corresponding *p*-H_2-enhanced signals now appear very clearly, while those of **3a** are suppressed, as expected, because of its high symmetry. Figure 9c shows the corresponding normal 32-scan ^{1}H NMR spectrum that was recorded under true Boltzmann conditions for comparison. These observations are therefore fully consistent with the expected redistribution of ligands in solution that allow the formation of an array of low-concentration species that are not readily detectable by normal NMR methods.

CONCLUSIONS

This study has revealed that when **3a**, **3b**, and **4a** are exposed to a solution containing H_2, pyridine, and acetonitrile, the dominant products are **3c** and **4c**. The ligand-exchange pathways of **3c** and **4c** were explored using EXSY methods. These studies revealed that **3c** undergoes preferential acetonitrile loss, while for **4c**, pyridine is lost preferentially. These processes are dissociative in nature and show the expected saturation behavior at high ligand concentrations. We further note that when a solution of **4a** is left under N_2, the CH bond activation product **5** is obtained.

Utilization of **3c** and **4c** as SABRE catalysts has also revealed that substantial enhancements in both pyridine and acetonitrile can be achieved. In this case, it is the chemical and magnetic inequivalence of the hydride ligands that provides the route to SABRE activity. This is reflected in these systems by both the axial and equatorial ligands seeing different hydride couplings and hence receiving SABRE transfer. The efficiency of the HP of free pyridine by **4a** is comparable with that of $Ir(COD)\{CO(CH_3)_2\}(IMes)]BF_4$. We note that in the case of **4a** the spin polarization derived from *p*-H_2 is now shared with just 7 in-plane protons, while in **2**, it is 12. Consequently, we confirm that one route to maximize the SABRE effect is to introduce fewer protons into the complex at the point of magnetization sharing. This effect overcomes its slower ligand-exchange rate compared to **2**. We also note that while **3** is better at polarizing acetonitrile, the reverse is true for **4**, with pyridine being

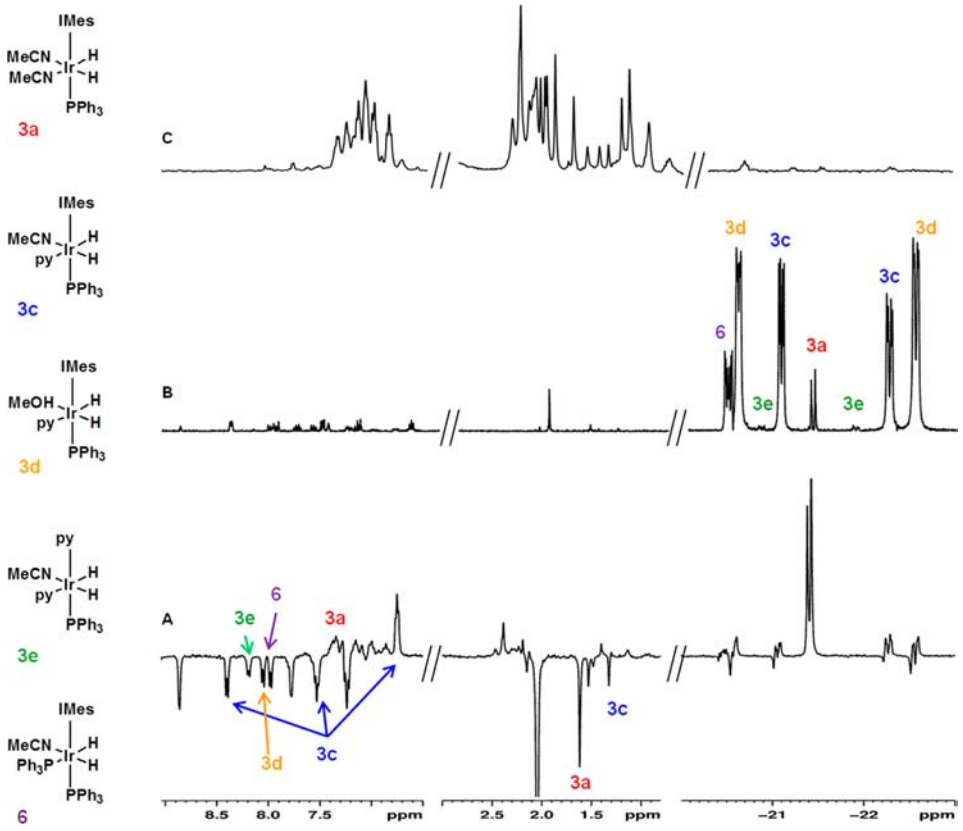

Figure 9. (a) ^{1}H NMR signals from hyperpolarized pyridine, PPh_3, the $-CH_3$ groups of IMes ligands, and the NCMe ligands that are detected as a consequence of SABRE. The enhanced signals in the hydride region are detected through PHIP. This NMR spectrum is the result of bubbling p-H_2 through a methanol-d_4 solution of **3c** at 130 G for 30 s prior to transfer into the NMR probe for observation. (b) Corresponding one-scan ^{1}H OPSY NMR spectrum of this sample. (c) Corresponding 32-scan ^{1}H NMR spectrum, recorded when the sample magnetization yields signals of an intensity that reflects the normal Boltzmann distribution rather than the HP conditions. The sample consisted of 3 mL of methanol-d_4 solution of **3c** (5.5 mM) and a 20-fold excess of pyridine.

optimally polarized. This observation is consistent with the change in the ligand-exchange mechanism, where **3** dissociates acetonitrile and **4** pyridine.

We have also shown that it is possible to detect hyperpolarized signals that are diagnostic of the ligands surrounding the metal centers through SABRE. In this case, $[Ir(H)_2(MeOH)(py)(IMes)(PPh_3)]BF_4$ (**3d**) and $[Ir(H)_2(NCMe)(py)_2(PPh_3)]BF_4$ (**3e**) were detected as a direct result of this process. These observations therefore illustrate a new route to using p-H_2-derived magnetization to characterize reaction intermediates. Two concepts have been explored here to aid this process. In the first, the effect of the magnetic field experienced by the sample at the point of polarization transfer has been examined and is related to the efficiency of ligand HP. These data revealed that it is possible to differentiate signals in the same NMR region by collecting a series of ^{1}H NMR spectra at different PTF values. We have also completed an extensive array of deuterium-labeling studies. These have confirmed that it is possible by reducing the extent of magnetization sharing to dramatically increase the level of transfer into the remaining ^{1}H sites in the catalyst system. This has been used not only to increase the level of pyridine and acetonitrile polarization but to aid in the characterization of the reaction intermediates **3d** and **3e**. We further note that when **3b** is formed as the isotopomer $[Ir(H)_2(h_5\text{-pyridine})(d_5\text{-pyridine})(IMes)(PPh_3)]BF_4$, the corresponding hydride ligand signals now become visible through PHIP rather than the SABRE effect. This is a direct consequence of the small chemical shift difference that exists between them and further illustrates how magnetic symmetry underpins both SABRE and PHIP observations.

Consequently, these measurements established that SABRE can be used to probe the NMR signature of the ligand sphere surrounding such hyperpolarized complexes. By utilizing the PTF to change the intensity of nearly overlapping resonances, it is possible to clearly distinguish them. We hope these examples help to illustrate a novel route to monitor reactivity. The results presented here also reveal how important it is to consider the role of all species present in solution when quantifying and explaining the appearance of SABRE-derived spectra.

■ ASSOCIATED CONTENT

Ⓢ Supporting Information

X-ray crystallographic data in CIF format and experimental details. This material is available free of charge via the Internet at http://pubs.acs.org.

■ AUTHOR INFORMATION

Corresponding Author

*E-mail: simon.duckett@york.ac.uk.

Author Contributions

All authors have given approval to the final version of the manuscript.

Funding

The authors thank Bruker Biospin UK for the p-H_2 polarizer used in this work. The EPSRC (Grant EP/G009546/1), Wellcome Trust (Grants 092506 and 098335), and University of York are also thanked for supporting this work.

Notes

The authors declare no competing financial interest.

■ ACKNOWLEDGMENTS

The Spanish MEC Consolider Ingenio 2010-ORFEO-CSD2007-00006 research programme is thanked. We thank Prof G. Green for helpful discussions and M. Buchner for help with the ^{19}F and ^{11}B NMR measurements.

■ REFERENCES

(1) Kurhanewicz, J.; Vigneron, D. B.; Brindle, K.; Chekmenev, E. Y.; Comment, A.; Cunningham, C. H.; DeBerardinis, R. J.; Green, G. G.; Leach, M. O.; Rajan, S. S.; Rizi, R. R.; Ross, B. D.; Warren, W. S.; Malloy, C. R. *Neoplasia* **2011**, *13*, 81.
(2) Bowers, C. R.; Weitekamp, D. P. *Phys. Rev. Lett.* **1986**, *57*, 2645.
(3) Bowers, C. R.; Weitekamp, D. P. *J. Am. Chem. Soc.* **1987**, *109*, 5541.
(4) Eisenschmid, T. C.; Kirss, R. U.; Deutsch, P. P.; Hommeltoft, S. I.; Eisenberg, R.; Bargon, J.; Lawler, R. G.; Balch, A. L. *J. Am. Chem. Soc.* **1987**, *109*, 8089.
(5) Heinrich, H.; Giernoth, R.; Bargon, J.; Brown, J. M. *Chem. Commun.* **2001**, 1296.
(6) Blazina, D.; Duckett, S. B.; Dyson, P. J.; Lohmann, J. A. B. *Chem.—Eur. J.* **2003**, *9*, 1045.
(7) Lopez-Serrano, J.; Duckett, S. B.; Aiken, S.; Lenero, K. Q. A.; Drent, E.; Dunne, J. P.; Konya, D.; Whitwood, A. C. *J. Am. Chem. Soc.* **2007**, *129*, 6513.
(8) Adams, R. W.; Duckett, S. B.; Green, R. A.; Williamson, D. C.; Green, G. G. R. *J. Chem. Phys.* **2009**, 131.
(9) Pravdivtsev, A. N.; Yurkovskaya, A. V.; Kaptein, R.; Miesel, K.; Vieth, H. M.; Ivanov, K. L. *Phys. Chem. Chem. Phys.* **2013**, *15*, 14660.
(10) Trantzschel, T.; Plaumann, M.; Bernarding, J.; Lego, D.; Ratajczyk, T.; Dillenberger, S.; Buntkowsky, G.; Bargon, J.; Bommerich, U. *Appl. Magn. Reson.* **2013**, *44*, 267.
(11) Roth, M.; Bargon, J.; Spiess, H. W.; Koch, A. *Magn. Reson. Chem.* **2008**, *46*, 713.
(12) Witte, C.; Schroder, L. *NMR Biomed.* **2013**, *26*, 788.
(13) Skovpin, I. V.; Zhivonitko, V. V.; Kaptein, R.; Koptyug, I. V. *Appl. Magn. Reson.* **2013**, *44*, 289.
(14) Kovtunov, K. V.; Beck, I. E.; Zhivonitko, V. V.; Barskiy, D. A.; Bukhtiyarov, V. I.; Koptyug, I. V. *Phys. Chem. Chem. Phys.* **2012**, *14*, 11008.
(15) Kovtunov, K. V.; Beck, I. E.; Bukhtiyarov, V. I.; Koptyug, I. V. *Angew. Chem., Int. Ed.* **2008**, *47*, 1492.
(16) Adams, R. W.; Aguilar, J. A.; Atkinson, K. D.; Cowley, M. J.; Elliott, P. I. P.; Duckett, S. B.; Green, G. G. R.; Khazal, I. G.; Lopez-Serrano, J.; Williamson, D. C. *Science* **2009**, *323*, 1708.
(17) Atkinson, K. D.; Cowley, M. J.; Elliott, P. I. P.; Duckett, S. B.; Green, G. G. R.; Lopez-Serrano, J.; Whitwood, A. C. *J. Am. Chem. Soc.* **2009**, *131*, 13362.
(18) Cowley, M. J.; Adams, R. W.; Atkinson, K. D.; Cockett, M. C. R.; Duckett, S. B.; Green, G. G. R.; Lohman, J. A. B.; Kerssebaum, R.; Kilgour, D.; Mewis, R. E. *J. Am. Chem. Soc.* **2011**, *133*, 6134.
(19) Duckett, S. B.; Mewis, R. E. *Acc. Chem. Res.* **2012**, *45*, 1247.
(20) Green, R. A.; Adams, R. W.; Duckett, S. B.; Mewis, R. E.; Williamson, D. C.; Green, G. G. R. *Prog. Nucl. Magn. Reson. Spectrosc.* **2012**, *67*, 1.
(21) Crabtree, R. H.; Felkin, H.; Morris, G. E. *J. Organomet. Chem.* **1977**, *141*, 205.
(22) Tolman, C. A. *Chem. Rev.* **1977**, *77*, 313.
(23) Perrin, L.; Clot, E.; Eisenstein, O.; Loch, J.; Crabtree, R. H. *Inorg. Chem.* **2001**, *40*, 5806.
(24) Huang, J. K.; Schanz, H. J.; Stevens, E. D.; Nolan, S. P. *Organometallics* **1999**, *18*, 2370.
(25) Chianese, A. R.; Li, X. W.; Janzen, M. C.; Faller, J. W.; Crabtree, R. H. *Organometallics* **2003**, *22*, 1663.
(26) Vazquez-Serrano, L. D.; Owens, B. T.; Buriak, J. M. *Inorg. Chim. Acta* **2006**, *359*, 2786.
(27) Brown, J. A.; Irvine, S.; Kennedy, A. R.; Kerr, W. J.; Andersson, S.; Nilsson, G. N. *Chem. Commun.* **2008**, 1115.
(28) Borowiak, R.; Schwaderlapp, N.; Huethe, F.; Lickert, T.; Fischer, E.; Baer, S.; Hennig, J.; von Elverfeldt, D.; Hoevener, J.-B. *Magn. Reson. Mater. Phys., Biol. Med.* **2013**, *26*, 491.
(29) van Weerdenburg, B. J. A.; Gloeggler, S.; Eshuis, N.; Engwerda, A. H. J.; Smits, J. M. M.; de Gelder, R.; Appelt, S.; Wymenga, S. S.; Tessari, M.; Feiters, M. C.; Blumich, B.; Rutjes, F. P. J. T. *Chem. Commun.* **2013**, *49*, 7388.
(30) Duecker, E. B.; Kuhn, L. T.; Muennemann, K.; Griesinger, C. *J. Magn. Reson.* **2012**, *214*, 159.
(31) Theis, T.; Ledbetter, M. P.; Kervern, G.; Blanchard, J. W.; Ganssle, P. J.; Butler, M. C.; Shin, H. D.; Budker, D.; Pines, A. *J. Am. Chem. Soc.* **2012**, *134*, 3987.
(32) Gloggler, S.; Emondts, M.; Colell, J.; Muller, R.; Blumich, B.; Appelt, S. *Analyst* **2011**, *136*, 1566.
(33) Gong, Q. X.; Gordji-Nejad, A.; Blumich, B.; Appelt, S. *Anal. Chem.* **2010**, *82*, 7078.
(34) Gloggler, S.; Muller, R.; Colell, J.; Emondts, M.; Dabrowski, M.; Blumich, B.; Appelt, S. *Phys. Chem. Chem. Phys.* **2011**, *13*, 13759.
(35) Ducker, E. B.; Kuhn, L. T.; Munnemann, K.; Griesinger, C. *J. Magn. Reson.* **2012**, *214*, 159.
(36) Lloyd, L. S.; Adams, R. W.; Bernstein, M.; Coombes, S.; Duckett, S. B.; Green, G. G. R.; Lewis, R. J.; Mewis, R. E.; Sleigh, C. J. *J. Am. Chem. Soc.* **2012**, *134*, 12904.
(37) Torres, O.; Martin, M.; Sola, E. *Organometallics* **2009**, *28*, 863.
(38) Tang, C. Y.; Smith, W.; Vidovic, D.; Thompson, A. L.; Chaplin, A. B.; Aldridge, S. *Organometallics* **2009**, *28*, 3059.
(39) Messerle, B. A.; Sleigh, C. J.; Partridge, M. G.; Duckett, S. B. *J. Chem. Soc., Dalton Trans.* **1999**, 1429.
(40) Plourde, P. V.; Dyroff, M.; Dukes, M. B. *Cancer Res. Treat.* **1994**, *30*, 103.